TÜBİTAK

Research Article

Turkish J. Eng. Env. Sci.
35 (2011) , 1 – 20.

doi:10.3906/muh-1005-32

Behaviour of elementary bolted steel T-stub connections: an evaluation of EC3 design procedure

Rabah SOLTANI*, Djamel Elddine KERDAL
Civil Engineering Department, Faculty of Architecture and Civil Engineering,
University of Sciences and Technology of Oran (Mohamed Boudiaf), BP.1505,
El Menaouar, 31000 Oran-ALGERIA
e-mail: rsoltanidz@yahoo.fr

Received: 19.05.2010

Abstract

Design rules of bolted steel beam-to-column connections have already turned towards new approaches in philosophy and methodology. In this paper, elementary bolted steel T-stub connections, proportioned according to Eurocode3 (EC3), were studied by means of a 3-dimensional finite element model using the ANSYS software package. The specimens reflected different geometric and strength parameters. Parameters considered were the thickness of the flange, the distance between the mid-web and the bolt line, and the distance between the bolt line and the end of the flange. The elastoplastic response, up to the ultimate state, was analysed and aspects relative to stiffness, strength, bolt loads, prying forces, and interaction between flanges were examined. Comparisons of experimental values, computed results, and EC3 predictions indicated that the design procedure still needs to be improved, owing to the complex phenomena embodied.

Key Words: Bolted steel T-stub connections, 3D finite elements, EC3 design procedure, combined failure modes, stiffness, strength, friction effects, contact region, prying forces, bolt loads

1. Introduction

Endplate bolted steel beam-to-column connections are widely used in steel structures. Their popularity is mainly attributed to the simplicity and economy associated with their fabrication and erection. However, their behaviour and analysis are quite complex. This complexity is due to the variation in geometric proportions, material properties, bolt preloading conditions, and many other factors, such as the induced curvatures in the endplate and column flange, and the distribution of the normal pressure and its associated contact regions between the flanges, which vary with changing load. In addition, analysis is generally complicated because of the number of components and their inherent combined nonlinear phenomena, like material and geometrical nonlinearities, friction, slippage, contact, and interaction.

*Corresponding author

1.1. Background to the study

Recently, design rules of bolted steel beam-to-column connections have turned towards new approaches in philosophy and methodology. In this context, one of the modern design codes (Eurocode3 (EC3), 2005) has introduced new design rules for beam-to-column bolted steel connections. For the case of endplate bolted steel connections with 4 bolts in the tension region and only 2 bolts in the compression region, as shown in Figure 1, the beam tension flange force is assumed to be transmitted over a small region of the endplate to the column flange, and the response of this portion can be represented by elementary bolted steel T-stub connections.

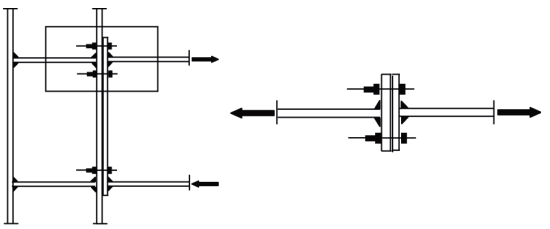

Figure 1. Endplate bolted steel beam-to-column connection with 4 bolts in tension region and 2 bolts in compression region.

According to the design procedure adopted by EC3, the yield failure modes of the tension region may occur by 1 of 3 typical failure modes, shown in Figure 2. These are plastic failure of the endplate or the column flange (mode 1), yielding of the endplate or column flange followed by bolt fracture (mode 2), or bolt fracture (mode 3). The corresponding failure modes are shown in Figures 2a-c, respectively. Studies in the inelastic regime have been concerned with formulae for the load carrying capacity or the minimum required thickness of the extended endplate and that of the column flange. The method of theoretical study most widely used and adopted by EC3 has been based upon yield line analysis using empirically determined straight or curved yield line patterns (Mansfield, 1957; Johansen, 1962). However, because of variation in proportions, different yield line patterns are associated with different yield line formulae and, therefore, lead to different strength capacities. In the elastic regime, studies were based on a simple theory of bending. However, to compute the elastic stiffness, EC3 applies a "geometric" model for whatever the proportions and bolt loading conditions are. Insofar as the prediction of the initial stiffness of the EC3 model is concerned, the preloading effects are disregarded in the model.

Endplate bolted steel beam-to-column connections in general, or the tension region in bolted steel beam-to-column connections in particular, has been the subject of substantial experimental research activity. Such studies (Douty and McGuire, 1965; Zoetemeijer, 1974; Agerskov, 1977; Packer and Morris, 1977; Moore and Sims, 1986; Grogan and Surtees, 1999; Swanson and Leon, 2001; Tagawa and Gurel, 2004) have included bare connections, welded transverse stiffeners, backing plates, and hot-rolled or cold-formed channels. In line with these developments, Bursi and Jaspart (1997) evaluated the degree of accuracy and limitations of EC3 design applications by testing and numerically analysing the behaviour of 2 elementary bolted steel T-stub connections, shown in Figure 3. The specimens were cut from IPE300 and HEB220 sections and their geometric characteristics are represented in Figures 3a and 3b, respectively. They were designed to fail according to the failure modes reported in Figures 2a and 2b, respectively. When comparing the load-displacement relationships of both the tested data and the EC3 predictions, the authors recognised that the EC3 model was unable to predict the load-displacement evolution and did not permit complete agreement between the predicted and test

data. To examine the degree of accuracy and limitations of the EC3 design procedure, Jaspart and Bursi (1997) also used 14 endplate steel beam-to-column connections bolted to a rigid base. Once again, the authors observed that the model underestimated the initial stiffness. However, it was stated that the design model was on the safe side as far as the plastic failure moments were concerned and that discrepancies were largely concentrated in thin endplates.

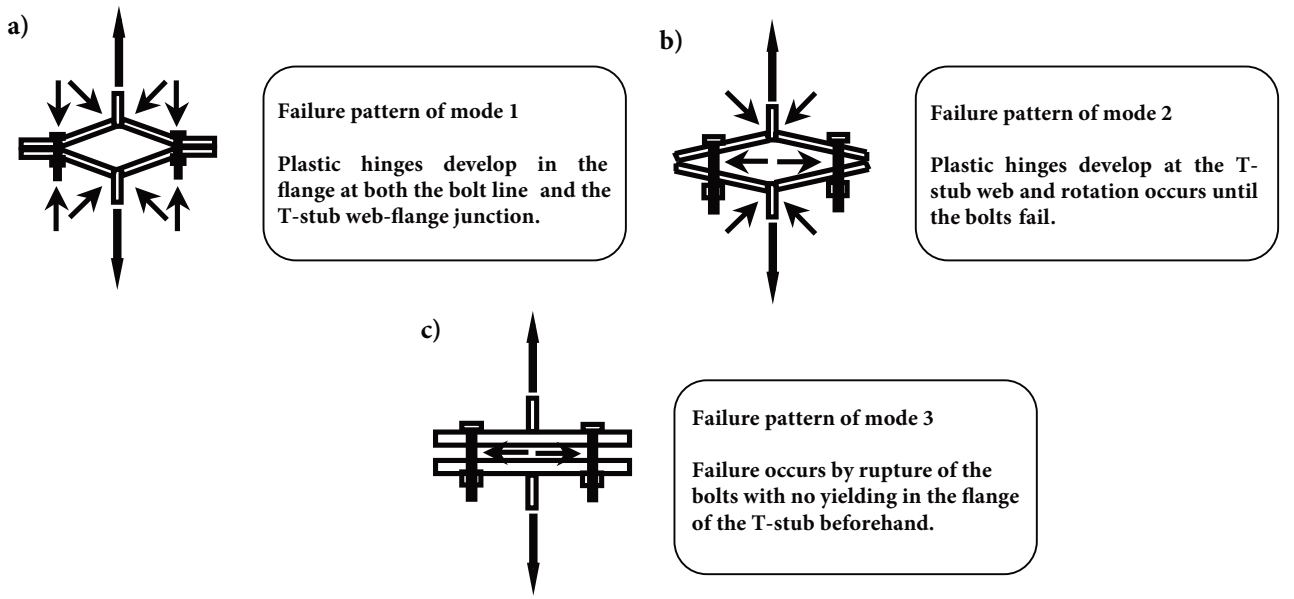

Note: Arrows indicate where plastic zones or failures are assumed to develop at plastic and ultimate limit.

Figure 2. Failure mode patterns of bolted steel T-stub connections according to EC3: a) failure mode 1, b) failure mode 2, c) failure mode 3.

Studies on bolted steel beam-to-column connections have also increasingly used finite element simulations (Bahaari and Sherbourne, 1994, 1997; Bursi and Jaspart, 1997; Jaspart and Bursi, 1997; Sherbourne and Bahaari, 1997; Bahaari and Sherbourne, 2000; Yang et al., 2000; Harada et al., 2003, Tagawa and Gurel, 2004). The results were fairly good within the range for which such validations were performed. However, since the bolted steel beam-to-column connections examined were statically indeterminate, the investigations were carried out to reproduce or predict the moment-rotation curve or, at least, to approximate the key parts of this relationship. In addition, although some research works have attempted finite element analyses, the design rules of EC3 are primarily based upon empirical studies.

As a modern code, EC3 should recognise that complete design of the tension region of bolted beam-to-column connections has, in any case, to consider much more than just the analysis of the yield line patterns with severe deformations and drastic assumptions at the failure limit state, or to reproduce or predict the moment-rotation relationship. One of the possibilities for improving the design procedure is to generate information on those aspects inherent to the behaviour of the tension region in bolted steel beam-to-column connections that cannot be provided from actual tests. The purpose of this paper is to examine the elastoplastic response of elementary bolted steel T-stub connections proportioned according to EC3 by means of a 3-dimensional finite element model using the ANSYS software package. Aspects relative to stiffness, strength, bolt loads, prying forces, and interaction between flanges were reviewed and a thorough study was made to provide some useful and relevant conclusions. Physical testing of 2 specimens considered by Jaspart and Bursi (1997) were adopted to

confirm the analysis and to adjust the models as necessary. Once adequate validation of the numerical analyses was established, the model could be used to generate information that could not be provided from actual tests. The findings obtained in this study are useful in checking the validity of the theoretical model being developed and will be adopted as a data basis in a subsequent paper.

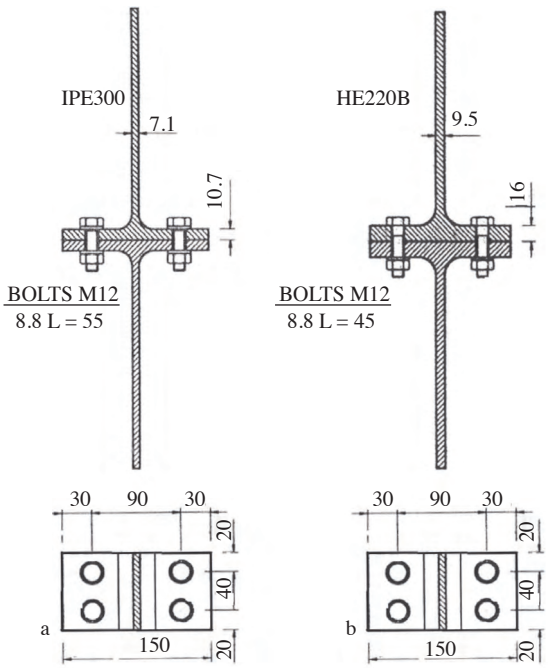

Figure 3. Geometrical characteristics of tested specimens (Bursi and Jaspart, 1997): a) IPE300 T-stub specimen, b) HEB220 T-stub specimen.

1.2. Approach of the study

The behaviour of endplate bolted steel beam-to-column connections is very complex and requires the consideration of various phenomena. Although the latest generation of research and commercial finite element codes is capable of simulating almost all of the complex phenomena outlined above, they require lengthy procedures and are very sensitive to the modelling options. To overcome this difficulty, the EC3 design approach uses the so-called component method, which supplies procedures for the evaluation of the global behaviour of the endplate bolted steel beam-to-column connections. In the case of endplate bolted steel connections with 4 bolts in the tension region and only 2 bolts in the compression region, the tension region represents an important component and is used for the evaluation of the strength capacity of the tension region and the initial stiffness. According to EC3, this component can be represented by an elementary bolted steel T-stub connection.

The study of elementary bolted steel T-sub connections is indeed appropriate as far as the behaviour of the tension region in the endplate bolted steel beam-to-column connections and their modes of failure are concerned. They are also relevant specimens as much knowledge can be derived from their behaviour, such as the interaction between the flanges and the distribution of the normal contact pressure induced by the normal stresses and in equilibrium with the prying force, initial stiffness, strength capacity, and bolt-induced load. Such aspects could be those inherent to the tension region in the endplate bolted steel beam-to-column connections.

Therefore, an understanding of these complex phenomena is of great benefit in setting a suitable basis upon which a theoretical model is to be developed and in which the connection will be able to reflect the assumptions used in analysis. This study can also be considered as a preliminary step to understanding the response of the tension region in endplate bolted steel beam-to-column connections.

The latest numerical approaches using the finite element technique have been shown to be capable of simulating almost all of the complex phenomena outlined above, and therefore analyses should be applied to investigate the complex phenomena in order to provide an accurate representation of the physics inherent to the tension region in endplate bolted steel beam-to-column connections. Relevant papers were reviewed to establish an appropriate approach for finite element simulation of the elementary bolted steel T-sub connections.

To gain insight into the behaviour of elementary bolted steel T-stub connections and examine some of the features outlined above, numerical simulations were performed on 44 nonpreloaded specimens involving various combinations of geometric and strength parameters and failure modes. Within each elementary bolted steel T-stub connection, the parameters considered were the distance between the mid-web thickness and the bolt line, and the distance between the bolt line and the end of the flange. Elastoplastic response, up to the ultimate state, was analysed and aspects relative to yield lines, interaction between flanges, prying forces, displacements, stiffness, and strength and bolt loads were examined. The computed values were compared with the EC3 model at each loading phase.

To reproduce the behaviour of the elementary bolted steel T-stub connections, numerical simulations were performed by 3D finite elements (FEs) using the ANSYS software package. To validate the proposed 3D FE model, comparisons were performed by superimposing the computed load-displacement relationships upon the measured ones (Bursi and Jaspart, 1997). The geometric properties of the 2 specimens (see Figure 3) are reported in Table 1 and the material data for the flanges and webs, i.e. the tensile value of yield stress and that of the tensile stress, are shown in Table 2. The bolts used were M12 grade 8.8 and characterised by the yield and ultimate stress values provided in Table 3.

Table 1. Geometric characteristics of bolted steel T-stub connections.

Cases	Specimens	a (mm)	b (mm)	t_f (mm)	t_w (mm)
1	IPE300	45	25 to 75	10.7	7.10
2	HEB220	45	25 to 75	16.0	9.50
3	IPE300	50	25 to 75	10.7	7.10
4	HEB220	50	25 to 75	16.0	9.50

Note: The distance b from the bolt line to the end of the T-stub flange was increased by 5 mm, starting from 25 mm and up to 75 mm.

2. Finite element model calibration

In pursuit of the above objectives, the ANSYS finite element software package was used. With this software package, the nonlinearities were performed according to Lagrange's formulation, which includes all kinematic effects due to large displacements and large strains. The 3D FE model, which reproduces the behaviour of the elementary bolted steel T-stub connections, incorporates simple contact elements to take into account conditions involving sticking, frictional sliding, and flange separation under large displacements. Friction is reproduced with a penalty method that makes the convergence of the solution more rapid at the expense of local solution

accuracy. A classical Coulomb friction model was used with 3 friction values (μ = 0, 0.25, and 0.50), and the Huber-von Mises-Hencky criterion was used to reproduce the plastic deformation in the bolted steel T-stub connections. In order to perform realistic simulations, the material data for flanges, webs, and bolt shanks were reproduced with piecewise constitutive linear stress-strain relationships.

Table 2. Strength properties of T-stub connections (Bursi and Jaspart, 1997).

Specimens	Yield stress f_y (MPa)	Tensile stress f_u (MPa)
IPE300		
Flange	431	595
Web	469	591
HEB220		
Flange	282	483
Web	290	498

Table 3. Strength properties of bolts (Bursi and Jaspart, 1997).

Specimens	Yield stress f_y (MPa)	Tensile stress f_u (MPa)
IPE300	893	974
HEB220	833	947

2.1. Convergence study

Prior to getting an insight into the performance of the specimens, several FE meshes were examined to determine the number of necessary elements for a reliable simulation and good predictions. The numerical convergence study was fulfilled by considering the specimens (Bursi and Jaspart, 1997) in the calibration process. As mentioned above, the specimens reflected different geometric and strength parameters. They were obtained from IPE300 and HEB220 sections and designed purposely to fail according to collapse modes 1 and 2, respectively (see Figures 2a and 2b).

Both specimens were doubly symmetric bolted steel T-stub connections in which the 2 opposite flanges were bolted together with 2 rows of bolts placed on each side of the web. To reduce the computing time, a quarter of each specimen was used, taking advantage of symmetry. Supports were provided to prevent any possible rigid displacements and the geometry of the bolt was modelled entirely with a head, a nut, and a cylindrical shank. The diameter of the shank was that of the nonthreaded one, and the data collected from physical testing (see Tables 1-3) were adopted in the calibration process. The thickness of the flange was discretised in a successive way by means of 1, 2, and 3 layers of elements. The mesh adopted was chosen on the basis of convergence studies. Figures 4a and 4b show the typical finite 3D element model adopted to reproduce the quarter of the IPE300 and HEB220 specimens, respectively, taking into account all of the assumptions stated previously. As a result, a 3-layer FE model was adopted to reproduce the complex kinematics dominated by the bending of the flange and to capture the stiffness and strength behaviour with good accuracy.

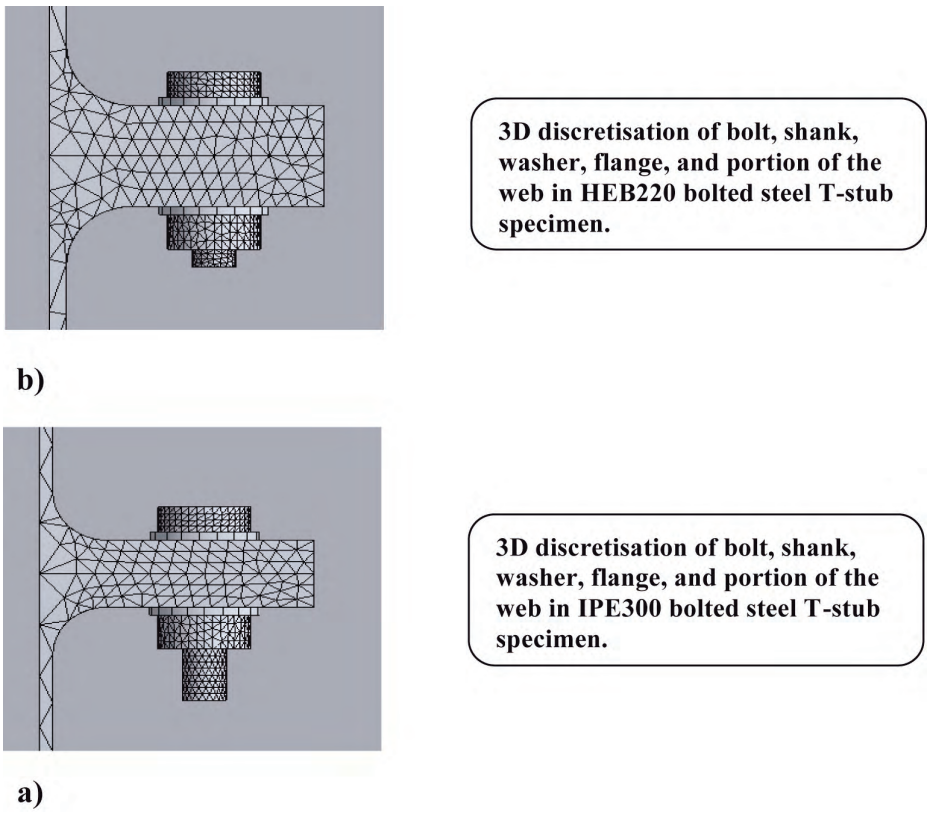

Figure 4. Finite element idealisation of T-stub connections: a) undeformed mesh of IPE300 specimen, b) undeformed mesh of HEB220 specimen.

2.2. Friction effect

To assess the sensitivity of the bolted steel T-stub connections to friction, 3 values (μ = 0, 0.25, and 0.50) were initially considered between the bolt washers and the flanges of the specimens and between the flanges of the elementary bolted steel T-stub connections. The accuracy of the model was quantified by superimposing the load-displacement relationships obtained by computed results and measured values. The load-displacement relationships were reproduced with good accuracy with the finite element code used, and the finite element model performed quite well for a practically stick condition (μ = 0.50) at the washer-flange interface with no friction between the flanges of both specimens. Zero friction between the flanges was traced to the symmetric behaviour of the specimens. The load-displacement relationships are shown in Figures 5a and 5b for both specimens.

It was shown that the finite element code presents similar curves in the elastic and virtually in large displacement regimes when compared with the measured ones. Friction effects were observed to slightly influence the elementary bolted steel stub connections in only the elastic regime. These final friction values were used to reproduce the load-displacement relationships of all of the specimens considered.

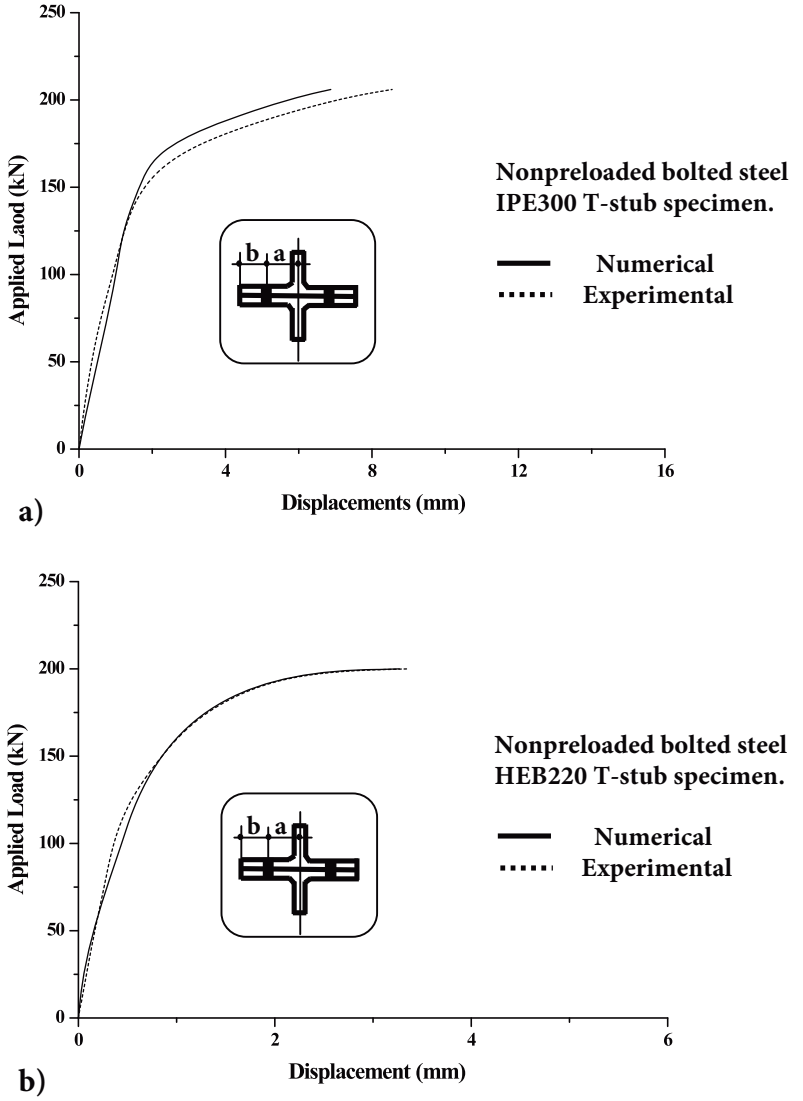

Figure 5. Experimental and computed load-displacement relationships: a) IPE300 T-stub specimen, b) HEB220 T-stub specimen.

3. Numerical results

3.1. Effect of distances a and b

Various studies have exposed the behaviour of the tension region in bolted steel beam-to-column connections. However, the large volume of information exposed did not address the potential interacting factors, such as the distance between the mid-web thickness and the bolt line (distance a) and the distance between the bolt line and the end of the elementary T-stub flange (distance b). The experimental approach is certainly the most popular, but it is time-consuming and expensive, and the data obtained are limited to surface measurements. As an alternative, the FE software package was adopted to analyse the elementary bolted steel T-stub connections using the 3D FE model, which was validated using physical test values. The 3D FE model was used to generate

information about these variables and to provide some useful and relevant information in order to improve the state of the current knowledge. We considered 4 cases, making a total of 44 nonpreloaded elementary bolted steel T-stub connections, and the geometric properties are summarised in Table 1. The top and bottom portions of the elementary bolted steel T-stubs were endowed with identical material and geometric properties.

The results of the numerically computed load-displacement relationships are shown in Figures 6a, 6b, 7a, and 7b, and the associated values are reported in Tables 4a, 4b, 5a, and 5b, respectively. The results included the specimens (Bursi and Jaspart, 1997) for which a = 45 mm and b = 30 mm. Figure 6 shows the load-displacement relationships for specimens IPE300 and HEB220, in which the distance between the mid-web thickness and the bolt line was given a constant value of 45 mm; the corresponding applied loads and computed displacements are listed in Tables 4a and 4b for specimens IPE300 and HEB220, respectively. Figure 7 also shows the load-displacement relationships for both specimens, in which the distance between the mid-web thickness and the bolt line was kept equal to 50 mm and the distance between the bolt line and the end of the flange varied from 25 mm to 75 mm at increments of 5 mm. The corresponding applied loads and computed displacements are shown in Tables 5a and 5b for specimens IPE300 and HEB220, respectively.

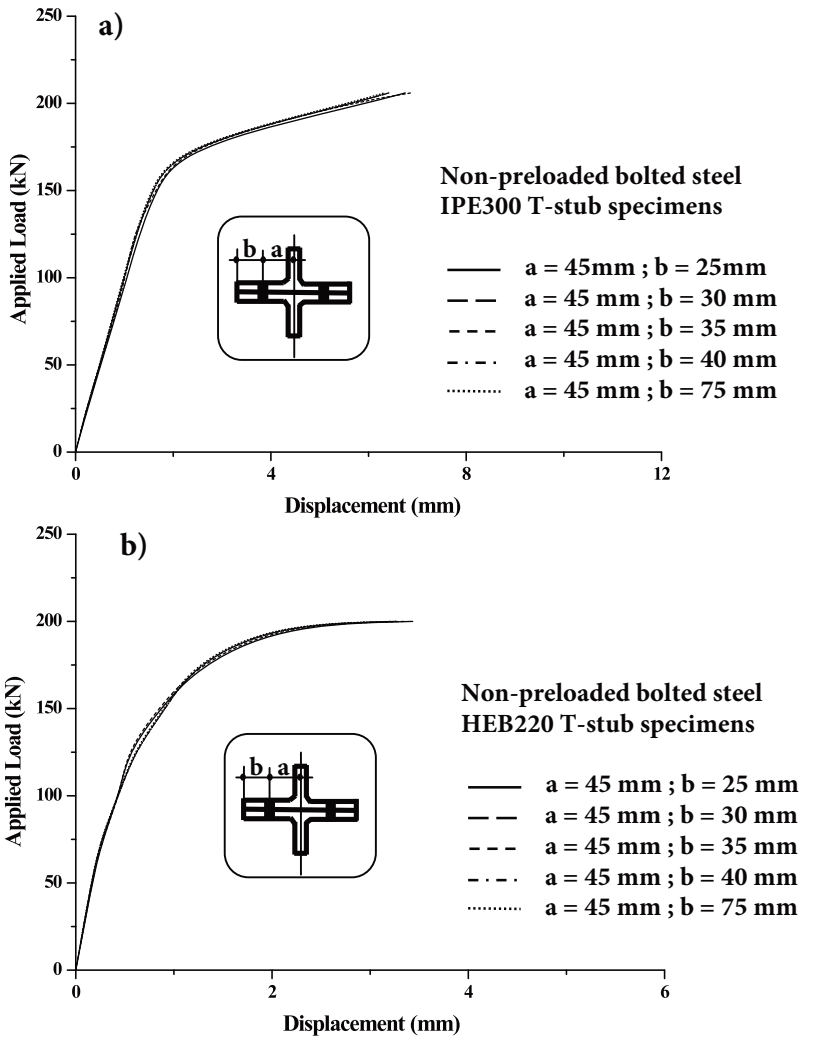

Figure 6. Effect of end-distance on load-displacement relationships: a) IPE300 specimens with a = 45 mm, b) HEB220 specimens with a = 45 mm.

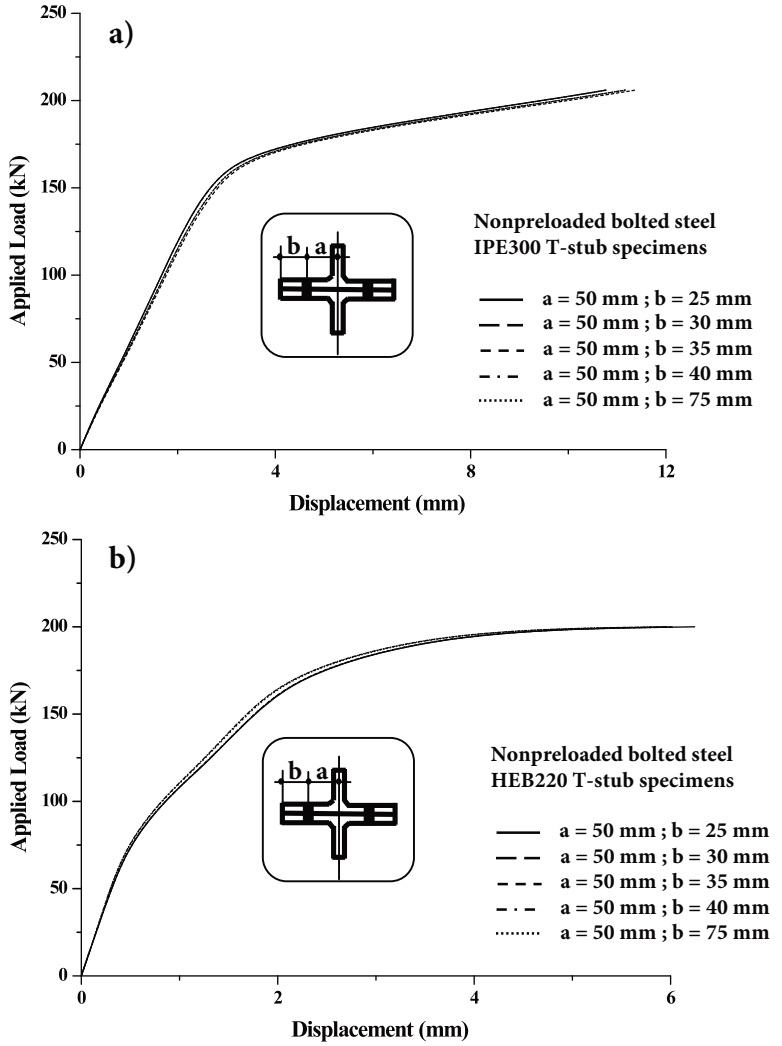

Figure 7. Effect of end-distance on load-displacement relationships: a) IPE300 specimens with a = 50 mm, b) HEB220 specimens with a = 50 mm.

Table 4a. Numerical and measured displacements for IPE300 specimens (a = 45 mm).

Load (kN)	b = 25 mm D (mm)	b = 30 mm D (mm)	b = 35 mm D (mm)	b = 40 mm D (mm)	b = 75 mm D (mm)
0	0.000	0.000/0.000	0.000	0.000	0.000
25	0.237	0.232/0.146	0.222	0.225	0.227
50	0.523	0.512/0.341	0.491	0.498	0.450
75	0.785	0.766/0.585	0.735	0.746	0.726
100	1.047	1.024/0.927	0.979	0.995	0.904
125	1.308	1.178/1.219	1.224	1.244	1.216
150	1.638	1.641/1.658	1.533	1.558	1.206
175	2.188	2.141/2.927	2.047	2.081	2.166
200	5.957	5.579/6.829	5.575	5.664	5.560
206	6.751	6.874/8.551	6.317	6.417	6.142

Note: The values on the right hand side in column 3 are measured values (Bursi and Jaspart, 1997).

Table 4b. Numerical and measured displacements for HEB220 specimens (a = 45 mm).

Load (kN)	b = 25 mm D (mm)	b = 30 mm D (mm)	b = 35 mm D (mm)	b = 40 mm D (mm)	b = 75 mm D (mm)
0	0.000	0.000/0.000	0.000	0.000	0.000
25	0.050	0.110/0.049	0.047	0.045	0.051
50	0.149	0.224/0.146	0.145	0.135	0.147
75	0.298	0.448/0.293	0.283	0.270	0.226
100	0.449	0.443/0.439	0.433	0.405	0.407
125	0.598	0.598/0.585	0.569	0.540	0.559
150	0.847	0.859/0.829	0.773	0.766	0.767
175	1.022	1.070/1.219	0.946	0.923	0.923
198	1.749	1.758/2.049	1.984	1.616	1.857
200	4.002	4.002/3.268	4.005	3.998	3.768

Note: The values on the right hand side in column 3 are measured values (Bursi and Jaspart, 1997).

Table 5a. Numerical displacements for IPE300 specimens (a = 50 mm).

Load (kN)	b = 25 mm D (mm)	b = 30 mm D (mm)	b = 35 mm D (mm)	b = 40 mm D (mm)	b = 75 mm D (mm)
0	0.000	0.000	0.000	0.000	0.000
25	0.378	0.401	0.392	0.379	0.392
50	0.835	0.882	0.866	0.836	0.866
75	1.252	1.324	1.299	1.255	1.299
100	1.671	1.765	1.732	1.673	1.732
125	2.087	2.206	2.165	2.091	2.165
150	2.614	2.762	2.711	2.618	2.711
175	3.491	3.689	3.621	3.496	3.621
198	9.505	10.051	9.858	9.522	9.858
200	10.771	11.381	11.171	10.791	11.172

Table 5b. Numerical displacements for HEB220 specimens (a = 50 mm).

Load (kN)	b = 25 mm D (mm)	b = 30 mm D (mm)	b = 35 mm D (mm)	b = 40 mm D (mm)	b = 75 mm D (mm)
0	0.000	0.000	0.000	0.000	0.000
25	0.152	0.152	0.146	0.145	0.152
50	0.305	0.304	0.293	0.291	0.299
75	0.491	0.489	0.471	0.467	0.485
100	0.833	0.831	0.801	0.794	0.787
125	1.331	1.327	1.277	1.267	1.259
150	1.751	1.744	1.681	1.666	1.767
175	2.295	2.288	2.203	2.186	2.183
198	3.871	3.859	3.716	3.687	3.857
200	6.246	6.227	5.996	5.948	5.768

The curves showed that larger distances between the mid-web thickness and bolt line decreased initial stiffness. By increasing distance b by 5 mm (i.e. from 45 mm to 50 mm), a mean value of 60% decrease in the

initial stiffness was obtained for the IPE300 specimens. When increasing this distance by the same value, the initial stiffness of the HEB220 specimens was decreased by only 33%. The results of the numerical simulations showed that each specimen was able to develop the same initial stiffness and strength capacity, both in the elastic and inelastic regimes, when the end distance was increased from 25 mm to 75 mm. From the analysis, it was observed that the stiffness and strength characteristics were not affected by the extension of end distance b as long as distance a remained constant. EC3 contains application rules for the evaluation of the effective length, which state that the maximum distance n between the bolt line and the point of application of the prying force cannot exceed 1.25 m or the distance b, i.e. n $\leq$ (1.25 m or b), whichever is smaller (1.25 m = 33.062 mm for IPE300 and 27.812 mm for HEB220). If only this specification is considered for comparison, then the considerations mean that the distance n, which gives the location of the point of application of the prying, does not exceed distance b as, beyond this value, the initial stiffness and the strength capacity will have the same values. In the following 2 sections, the FE analyses presented were restricted to the specimens with distance b varying from 25 mm to 40 mm only.

3.2. Prying action

For an insight into the evolution of the contact regions, the amplitudes, and the location of the normal pressure distribution and to quantify the effective line of action of the prying force, FE analyses were also done for the same 44 nonpreloaded specimens. Results are shown for a few of them, for the reasons stated above. The corresponding elastoplastic prying force values are presented in Tables 6a-d for IPE300 specimens and Tables 7a-d for HEB220 specimens.

To compute the prying force, it was expedient to consider the mean stresses and the corresponding effective contact regions participating in the action. The computed values of prying forces with their respective ratios are reported in columns 5-7. Prying forces using the EC3 model are displayed in column 6 for direct comparisons. These show that the design model gave smaller values but that discrepancies were larger in specimens with an increasing distance b. One also has to notice that the EC3 model predicts prying force values only in the elastic regime.

Table 6a. Numerical and EC3 values for IPE300 specimen (a = 45 mm and b = 25 mm).

F (kN)	B_{nu} (kN)	B_{ec} (kN)	B_{nu}/B_{ec}	Q_{nu} (kN)	Q_{ec} (kN)	Q_{nu}/Q_{ec}
0	0.000	0.000	-	0.000	0.000	-
25	9.574	9.119	1.05	2.918	2.869	1.02
50	18.103	18.239	0.99	5.848	5.739	1.02
75	27.712	27.358	1.01	8.778	8.608	1.02
100	36.296	36.477	1.05	11.672	11.477	1.02
125	46.833	45.597	1.03	14.152	14.347	0.99
150	55.476	54.716	1.01	17.535	17.216	1.02
175	62.119	*	-	19.684	*	-
200	70.102	*	-	23.407	*	-
206	76.762	*	-	26.055	*	-

Note: Asterisks indicate that the inelastic values were not covered in the EC3 model.

Table 6b. Numerical and EC3 values for IPE300 specimen (a = 45 mm and b = 30 mm).

F (kN)	B_{nu} (kN)	B_{ec} (kN)	B_{nu}/B_{ec}	Q_{nu} (kN)	Q_{ec} (kN)	Q_{nu}/Q_{ec}
0	0.000	0.000	-	0.000	0.000	-
25	9.387	8.540	1.10	3.007	2.290	1.31
50	18.182	17.080	1.06	6.015	4.580	1.31
75	27.773	25.620	1.08	8.222	6.870	1.20
100	36.364	34.160	1.06	11.029	9.160	1.20
125	45.520	42.700	1.07	13.437	11.450	1.17
150	53.694	51.241	1.05	16.044	13.741	1.17
175	64.320	*	-	19.570	*	-
200	69.650	*	-	21.277	*	-
206	77.875	*	-	25.754	*	-

Note: Asterisks indicate that the inelastic values were not covered in the EC3 model.

Table 6c. Numerical and EC3 values for IPE300 specimen (a = 45 mm and b = 35 mm).

F (kN)	B_{nu} (kN)	B_{ec} (kN)	B_{nu}/B_{ec}	Q_{nu} (kN)	Q_{ec} (kN)	Q_{nu}/Q_{ec}
0	0.000	0.000	-	0.000	0.000	-
25	8.574	8.133	1.05	2.363	1.883	1.29
50	18.103	16.267	1.11	4.725	3.767	1.25
75	26.712	24.400	1.09	7.808	5.650	1.38
100	35.296	32.533	1.08	9.467	7.533	1.26
125	43.833	40.667	1.08	11.873	9.417	1.26
150	52.476	48.800	1.07	15.360	11.300	1.36
175	62.119	*	-	18.564	*	-
200	75.102	*	-	21.230	*	-
206	77.762	*	-	25.154	*	-

Note: Asterisks indicate that the inelastic values were not covered in the EC3 model.

Table 6d. Numerical and EC3 values for IPE300 specimen (a = 45 mm and b = 40 mm).

F (kN)	B_{nu} (kN)	B_{ec} (kN)	B_{nu}/B_{ec}	Q_{nu} (kN)	Q_{ec} (kN)	Q_{nu}/Q_{ec}
0	0.000	0.000	-	0.000	0.000	-
25	8.387	8.015	1.04	2.902	1.765	1.64
50	17.182	16.029	1.07	5.095	3.529	1.44
75	25.773	24.044	1.07	7.160	5.294	1.35
100	34.364	32.058	1.07	12.225	7.059	1.73
125	43.520	40.074	1.08	15.434	8.824	1.75
150	53.694	48.088	1.12	17.170	10.588	1.62
175	62.320	*	-	23.206	*	-
200	73.650	*	-	25.405	*	-
206	77.875	*	-	26.559	*	-

Note: Asterisks indicate that the inelastic values were not covered in the EC3 model.

Table 7a. Numerical and EC3 values for HEB220 specimen (a = 45 mm and b = 25 mm).

F (kN)	B_{nu} (kN)	B_{ec} (kN)	B_{nu}/B_{ec}	Q_{nu} (kN)	Q_{ec} (kN)	Q_{nu}/Q_{ec}
0	0.000	0.000	-	0.000	0.000	-
25	9.174	9.119	1.01	2.718	2.869	0.95
50	18.003	18.239	0.99	5.488	5.739	0.96
75	27.172	27.358	0.99	8.778	8.608	1.02
100	36.692	36.477	1.01	11.267	11.477	0.98
125	46.833	45.597	1.03	14.152	14.347	0.99
150	55.476	54.716	1.01	17.135	17.216	0.99
175	64.119	*	-	21.684	*	-
198	61.102	*	-	20.407	*	-
200	77.267	*	-	25.055	*	-

Note: Asterisks indicate that the inelastic values were not covered in the EC3 model.

Table 7b. Numerical and EC3 values for HEB220 specimen (a = 45 mm and b = 30 mm).

F (kN)	B_{nu} (kN)	B_{ec} (kN)	B_{nu}/B_{ec}	Q_{nu} (kN)	Q_{ec} (kN)	Q_{nu}/Q_{ec}
0	0.000	0.000	-	0.000	0.000	-
25	9.387	8.540	1.10	2.667	2.290	1.16
50	17.982	17.080	1.05	5.015	4.580	1.09
75	26.773	25.620	1.04	8.222	6.870	1.20
100	36.364	34.160	1.06	11.229	9.160	1.22
125	45.520	42.700	1.07	14.137	11.450	1.23
150	54.694	51.241	1.07	16.044	13.741	1.17
175	64.320	*	-	19.057	*	-
198	69.650	*	-	21.277	*	-
200	77.875	*	-	25.754	*	-

Note: Asterisks indicate that the inelastic values were not covered in the EC3 model.

Table 7c. Numerical and EC3 values for HEB220 specimen (a = 45 mm and b = 35 mm).

F (kN)	B_{nu} (kN)	B_{ec} (kN)	B_{nu}/B_{ec}	Q_{nu} (kN)	Q_{ec} (kN)	Q_{nu}/Q_{ec}
0	0.000	0.000	-	0.000	0.000	-
25	8.387	8.133	1.05	2.902	1.883	1.44
50	17.182	16.267	1.11	5.095	3.767	1.57
75	25.773	24.400	1.09	7.379	5.650	1.31
100	34.364	32.533	1.08	12.939	7.533	1.72
125	43.520	40.667	1.08	15.098	9.417	1.60
150	53.694	48.800	1.07	17.460	11.300	1.55
175	62.320	*	-	23.164	*	-
198	73.650	*	-	25.530	*	-
200	77.875	*	-	26.554	*	-

Note: Asterisks indicate that the inelastic values were not covered in the EC3 model.

Table 7d. Numerical and EC3 values for HEB220 specimen (a = 45 mm and b = 40 mm).

F (kN)	B_{nu} (kN)	B_{ec} (kN)	B_{nu}/B_{ec}	Q_{nu} (kN)	Q_{ec} (kN)	Q_{nu}/Q_{ec}
0	0.000	0.000	-	0.000	0.000	-
25	8.387	8.015	1.05	2.702	1.765	1.53
50	17.182	16.029	1.07	5.895	3.529	1.67
75	25.773	24.044	1.07	7.360	5.294	1.39
100	34.364	32.058	1.07	12.125	7.059	1.72
125	43.520	40.074	1.09	15.934	8.824	1.80
150	53.694	48.088	1.12	18.170	10.588	1.72
175	62.320	*	-	22.206	*	-
198	73.650	*	-	25.405	*	-
200	77.875	*	-	26.559	*	-

Note: Asterisks indicate that the inelastic values were not covered in the EC3 model.

The finite element analyses were also able to show the evolution of the normal pressure distribution. However, for the sake of brevity, only comments are given in this section. For all specimens, when distance b was increased beyond 40 mm, the portion of the flanges between this limit and the ends was contact- or pressure-free, and the size of this portion increased with the increase of distance b. Thus, as far as the specimens considered herein are concerned, the limit line of action of the prying force remained unchanged beyond this distance (b = 40 mm).

In examining the evolution of the normal pressure distribution in the specimens, there appeared to be a relation between distance b and the thickness of the flange. Therefore, as the load increased, the evolution of the pressure in the contact region between the flanges changed both in magnitude and location due to flexure and prying force. For instance, in the case of the specimens with a 16-mm flange thickness (HEB220), the flexure stiffness of the flange appeared to cause the prying force to develop at the end of the flange, both in the elastic and plastic regimes.

In detail, when distance b was 25 mm, the prying force exerted pressure right at the end of the flange. When this distance was increased to 40 mm, although the normal pressure distribution spread a little over a limited area towards the bolt, it was still concentrated at the end of the flange. With specimens having a flange thickness of 10.7 mm (IPE300), the normal pressure generated by the normal stresses in equilibrium with the prying force was well localised near the end of the flange up to the yielding onset, and then the contact region was enlarged, in a progressive manner, towards the bolt line.

3.3. Bolt-induced loads

Finite element analyses also permitted the computation of the bolt forces induced at each load step. To examine the discrepancies between the EC3 model and the computed values, the simulation process was applied to all of the specimens. A rigorous stress analysis was performed. The corresponding results with their respective ratios are reported in columns 2-4 of Tables 6a-d and 7a-d for the IPE300 and HEB220 specimens, respectively. Bolt loads using the EC3 model are also given in column 3 for direct comparisons. One can conclude that lesser discrepancies were observed for the bolt-induced loads produced by the numerical analyses and those of the EC3 model. Once again, one has to notice that the EC3 model predicted values for bolt-induced loads only in the elastic regime.

3.4. Effect of combined failure modes

The objective of this section is to examine the complex behaviour of nonpreloaded bolted steel T-stub connections with combined failure modes. Different specimens were considered, involving a combination of geometric and strength properties and failure modes. The general layout of the specimens is illustrated in Figure 8 and the geometric and strength parameters of the specimens are reported in Tables 2, 3, and 8.

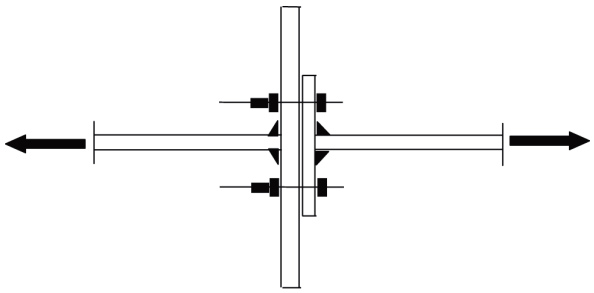

Figure 8. Typical layout of specimens used in combined failure mode.

Table 8. Geometric characteristics of bolted steel T-stub connections.

Specimens	Case 1	Case 2	Case 3	Case 4
a = 45 mm				
Top half T-stub	IPE300	IPE300	IPE300	IPE300
b = 30 mm				
a = 45 mm				
Bottom half T-stub	IPE300	HEB220	IPE300*	IPE300*
b = 30, 35, 40, and 75 mm				

Note: Asterisks indicate that the flange and web strength values were those of HEB220 (case 3); half of the flange thickness of IPE300 was used for the bottom flange (case 4).

As indicated in Table 8, 4 cases of elementary bolted steel T-stub connections were considered. In some specimens, the top T-stub flanges were made shorter than the bottom ones to simulate the case of short T-stubs bolted to long column flanges. All specimens were endowed with a distance a of a constant value of 45 mm. The top flanges were designed to fail according to mode 1 and had a constant distance a of 30 mm. The bottom flanges of specimens in cases 1 and 2 were designed to fail according to mode 1 and mode 2, respectively, and had 3 values for the distance between the mid-web thickness and bolt line (a = 30, 40, and 75 mm). Specimens in case 3 were identical to those of case 1, but the bottom webs and flanges had the strength values of HEB200 specimens. Finally, in case 4, the specimens were similar to those of case 1, except that the flange thickness of the bottom T-stubs was half that of the top one.

The numerical analyses were carried out both in elastic and plastic regimes. For the sake of brevity, the results are given only for the plastic regime, where the behaviour of the T-stub flanges is characterised by large displacement and stress fields, and from which one can better visualise the flange kinematics and corresponding interactions. The displacement and stress fields at the plastic failure state traced by the FE analysis are illustrated in Figures 9 and 10, and the results presented here are restricted to load F = 200 kN.

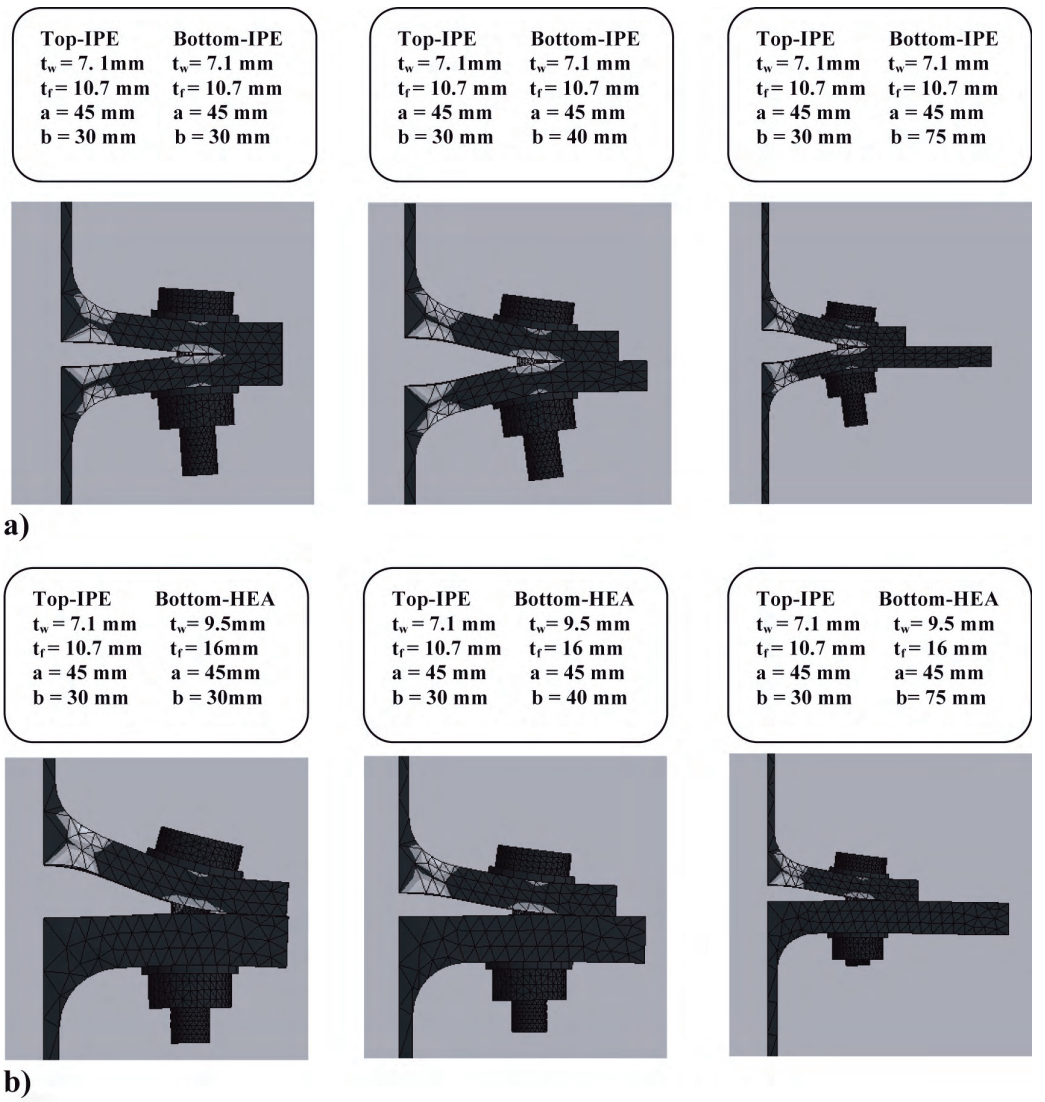

Figure 9. Illustrations of complex behaviour of specimens endowed with different geometric, strength, and failure modes.

The deformed shapes and the corresponding distributions of the von Mises equivalent stresses of the 3 specimens of case 1, with identical top and bottom flange thicknesses (t_f = 10.7 mm), are illustrated in Figure 9a. One can observe that the yield lines developed, in both top and bottom flanges, near the bolt line and at the toe of the fillet. The 2 yield lines governed the failure mode observed, which agreed with failure mode 1 predicted by EC3 and shown in Figure 2a. FE results were also reproduced for the 3 specimens considered in case 2, which had identical top T-stub flanges (t_f = 10.7 mm), as in case 1. However, the bottom T-stub flanges had thicknesses of 16 mm (t_f = 16 mm). The effect of the bottom flange thickness on the distribution of von Mises equivalent stresses is shown in Figure 9b. Such a distribution clearly mirrors the fact that only the top T-stubs with thin flanges were influenced by high stress levels. Again, the yield lines were formed, in the top flange, near the bolt line and at the toe of the fillet. Specimens of case 3 were similar to those of case 1, with the exception that the strength values of the HEB220 specimens were implemented for the bottom T-stub flanges. For these specimens, yielding was formed only in the bottom flange, although both top and bottom flanges had

the same thickness, as shown in Figure 10a. In addition, the plastic deformations were concentrated in a line pattern at the toe of the fillet and spread around the bolt hole. One can also observe that plasticity reached the bottom T-stub webs. Finally, the displacement and von Mises equivalent stress fields of the specimens of case 4 are illustrated in Figure 10b. The 3 specimens performed in 3 different ways. In one case (left), no plastic deformation was observed, although it was expected that the bottom flange, which had a flange thickness of 5.35 mm (t_f = 5.35 mm), would be influenced by the high stress level. These aspects did not agree with either of the failure modes predicted by EC3. For the specimens with a larger bottom flange (b = 40 mm), one can observe that the yield lines developed only in the bottom flange, near the bolt line and at the toe of the fillet (middle). Lastly, from the distribution of the von Mises equivalent stresses and the corresponding deformed shapes of specimens with the longest bottom flange (b = 75 mm), one can observe that the yield lines still developed in the bottom flange. However, plastic deformation was also present at the top flange, but only at the toe of the fillet (right). Again, this did not agree with failure mode 1 predicted by EC3.

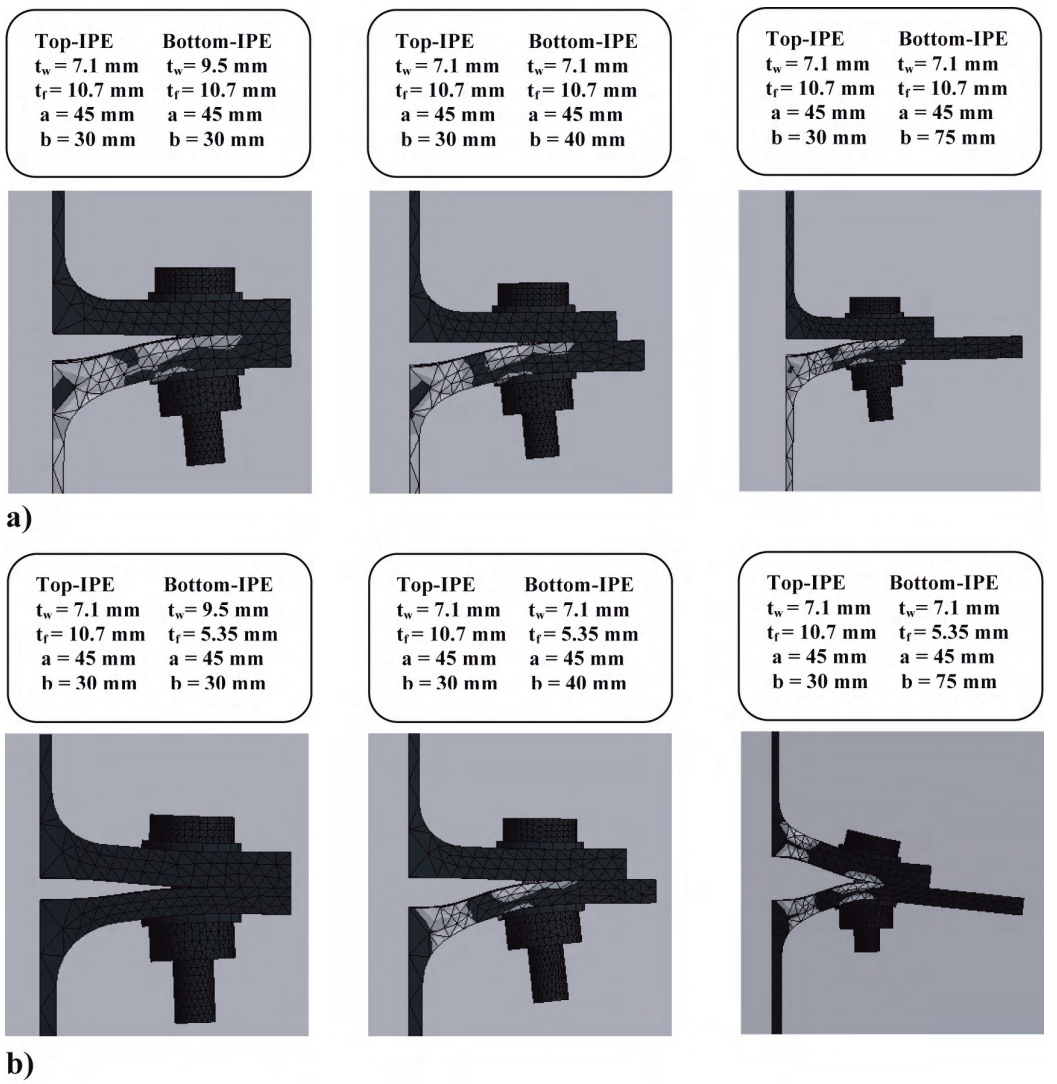

Figure 10. Illustrations of complex behaviour of specimens endowed with different geometric, strength, and failure modes.

As illustrated, the specimens performed in different ways under combined failure modes and different geometric and strength parameters. Although the observed displacement and stress distribution fields resulting from the FE model were related to elementary bolted steel T-stub connections, features like this could be those inherent to the tension region in endplate bolted steel beam-to-column connections. An understanding of these complex phenomena is of great benefit in setting a suitable basis upon which to develop a theoretical model and in which the connection will be able to reflect the assumptions used in analysis.

4. Conclusion

This study was devoted to the analysis of elementary bolted steel T-stub connections by a 3D finite element model using the ANSYS software package. The elementary bolted steel T-stub connections used were endowed with different geometric and strength parameters as well as failure modes. The 3D FE model was able to reproduce the elastoplastic response, up to the ultimate state, and aspects such as stiffness, strength, bolt loads, and prying forces were examined. The comparisons performed highlighted discrepancies between numerical results and the EC3 model. It was concluded that the EC3 design procedure still needs to be improved and that a rigorous model is required. In this paper, aspects relative to elementary bolted steel T-stub connections were studied. A theoretical model to predict the behaviour of nonpreloaded elementary bolted steel T-stub connections will be presented in a subsequent paper in the same journal. Numerical results obtained from the finite element simulations will be included to demonstrate the validity of the model.

Acknowledgement

The authors express their gratitude to the laboratory staff of Applied Mechanics, Department of Mechanical Engineering, Faculty of Mechanical Engineering and Metallurgy, University of Sciences and Technology, Mohamed BOUDIAF, Oran, Algeria.

References

Agerskov, H., "Analysis of Bolted Connections Subject to Prying", Journal of the Structural Division, 103, 2145-2163, 1977.

Bahaari, M.R. and Sherbourne, A.N., "3D Simulation of Endplate Bolted Connections", Journal of Structural Engineering, 120, 3122-3136, 1994.

Bahaari, M.R. and Sherbourne, A.N., "3D Simulation of Bolted Connections to Unstiffened Columns: Extended Endplate Connections", Journal of Constructional Steel Research, 40, 189-223, 1997.

Bahaari, M.R. and Sherbourne, A.N., "Behaviour of Eight Bolt Large Capacity Endplate Connections", Computers and Sciences, 77, 315-325, 2000.

Bursi, O.S. and Jaspart, J.P., "Benchmarks for Finite Element Modelling of Bolted Steel Connections", Journal of Constructional Steel Research, 43, 17-42, 1997.

Douty, R.T. and McGuire, W., "High Strength Bolted Moment Connections", Journal of the Structural Division, 91, 101-128, 1965.

Eurocode3, Design of Steel Structures: General Rules and Rules for Buildings, Brussels, Belgium, 2005.

Grogan, W. and Surtees, J.O., "Experimental Behaviour of Endplate Connections Reinforced with Bolted Backing Angles", Journal of Constructional Steel Research, 50, 71-96, 1999.

Harada, Y., Nagawa, H. and Morita. K., "Out-of-Plane Behaviour of Column Skin Plate in RHS Column-to-Split-T Tensile Connection with High Strength Bolts", Journal of Structural and Construction Engineering, 56, 173-180, 2003.

Jaspart, J.P. and Bursi, O.S., "Calibration of a Finite Element Model for Isolated Bolted Endplate Steel Connections", Journal of Constructional Steel Research, 44, 225-262, 1997.

Johansen, K.W., Yield Line Theory, Cement and Concrete Association, London, 1962.

Mansfield, E.H., Studies in Collapse Analysis of Rigid Plastic Plates With a Square Yield Diagram, London, 1957.

Moore D.B. and Sims, P.A.C., "Preliminary Investigations into the Behaviour of Extended Endplate Steel Connections with Backing Plates", Journal of Constructional Steel Research, 6, 95-122, 1986.

Packer, J.A. and Morris, L.J., "A Limit State Design Method for Tension Region of Bolted Beam-Column Connections", The Structural Engineer, 55, 446-458, 1977.

Sherbourne, A.N. and Bahaari, M.R., "3D Simulation of Bolted Connections to Unstiffened Columns: T-stub Connections", Journal of Constructional Steel Research, 40, 169-187, 1997.

Swanson, J.A. and Leon, R.T., "Bolted Steel Connections: Tests on T-stub Components", Journal of Structural Engineering, 127, 498-512, 2001.

Tagawa, H. and Gurel, S., Strength Evaluation of Bolted Moment Connections Stiffened With Channels, Tokai, Japan, 2004.

Yang, J.G., Murray, T.M and Plaut, R.H., "Three Dimensional Finite Element Analysis of Double Angle Connections under Tension and Shear", Journal of Constructional Steel Research, 54, 227-244, 1997.

Zoetemeijer, P., A Design Method for the Tension Side of Statically Loaded Bolted Beam to Column Connections, Delft, Netherlands, 1974.